Materials and Design 191 (2020) 108605

Contents lists available at ScienceDirect

Materials and Design

journal homepage: www.elsevier.com/locate/matdes

An analysis of fatigue failure mechanisms in an additively manufactured and shot peened IN 718 nickel superalloy

Enrico Salvati [a,*], Alexander J.G. Lunt [b], Chris P. Heason [c], Gavin J. Baxter [c], Alexander M. Korsunsky [a]

[a] MBLEM, Department of Engineering Science, University of Oxford, Parks Road, Oxford OX1 3PJ, UK
[b] Department of Mechanical Engineering, University of Bath, Claverton Down, Bath BA2 7AY, UK
[c] Rolls-Royce plc, P.O. Box 31, Derby DE24 8BJ, UK

HIGHLIGHTS

- Fatigue microstructural characteristics and presence of residual stress in additively manufactured IN718 were studied.
- Fatigue cracks originated at the surface of large internal material defects (i.e. void).
- Twinning deformation was found to be the dominant deformation mechanism during fatigue crack propagation · A high concentration of Chromium was found at the defect where crack nucleation occurred.
- Shot peening was found to be detrimental in this instance due to the tensile residual stress in the bulk of the material

GRAPHICAL ABSTRACT

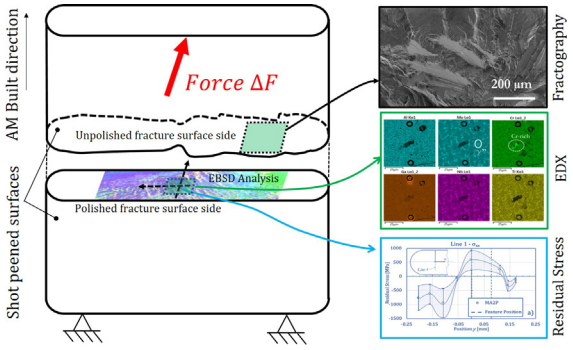

ARTICLE INFO

Article history:
Received 8 January 2020
Received in revised form 3 February 2020
Accepted 25 February 2020
Available online 26 February 2020

Keywords:
Additive manufacturing
Direct energy deposition
IN718
Residual stress
Twinning
Fatigue

ABSTRACT

The family of additive manufacturing techniques has been attracting significant attention of manufacturers and researchers, due to its unrivalled flexibility to fabricate and repair geometrically complex objects. However, material shaping is not sufficient: wide adoption of additive manufacturing can only occur upon the achievement of satisfactory mechanical performance in terms of structural integrity. The present study exploits a wide range of micro-scale experimental techniques to shed light on fatigue failure mechanisms of Laser Metal Deposition IN718 Ni-base superalloy, and to study the effect of shot peening treatment. Thorough microstructural and fractographic analyses revealed the main deformation mechanism associated with twinning during crack propagation, while crack initiation was found to be promoted by both slip system deformation and twinning around microstructural defects, rather than at sample free-surfaces. It was found that precipitates played a major role in determining the deformation mode. It was discovered that in this case-study, shot-peening residual stresses may have a detrimental effect, in view of the presence of the largest defects within a region where tensile residual stress was present. The results presented here improve understanding of failure mechanisms and thus define future directions of development for manufacture optimisation.

1. Introduction

In contrast with traditional manufacturing processes in which material subtraction approach is employed for the production of mechanical

* Corresponding author at: Department of Engineering Science, University of Oxford, Parks Road, Oxford OX1 3PJ, UK.
E-mail address: enrico.salvati@eng.ox.ac.uk (E. Salvati).

https://doi.org/10.1016/j.matdes.2020.108605

components, Additive Manufacturing (AM) relies on the layer-by-layer material build-up [1]. Although this technique has now been explored for a couple of decades, only recently it has began to emerge as a manufacturing technique that can be potentially incorporated in mainstream production of high-performance metallic components in industries such as aerospace. The constantly growing popularity of AM is driven by its unique capability for manufacturing geometrically complex three-dimensional parts. The adoption of AM must also be considered in the context of its cost-effectiveness compared to conventional manufacturing routes [2].

AM can be thought of as a repeated welding process in which strong thermal gradients are necessarily involved [3]. The material is rapidly heated above the melting temperature by an the electron or laser beam, which is followed by rapid cooling by heat conduction, and solidification as the heat source moves away. Given the nature of the process, the heat source returns for a short period of time to the zone where the material has solidified, and therefore numerous re-heating and re-cooling processes occur, analogously to repeating thermal treatments. Since the material microstructure in general is highly dependent on thermal history, the resulting microstructure may be of considerably different nature compared to classic manufacturing processes (e.g. casting). In fact, the presence of high temperature gradients may introduce gradients of phases throughout the manufactured part [4], and often meta-stable phases can form, which are produced in conventional processes, closer to equilibrium. An additional important consequence of the material thermal history is the developing of porosity and defect population which is well known to be detrimental from a structural integrity perspective [5–8]. Given the complex thermal history involved in AM, another consequence worth considering is the generation of Residual Stress (RS) at different length scales [9,10]. These may be amplified if the material being manufactured shows a significant degree of anisotropy in terms of the mechanical and thermal properties. RS is well known to affect material structural integrity, particularly when the external loads are of cyclic manner (i.e. fatigue) [11–13]. In High Cycle Fatigue (HCF) particularly, crack nucleation takes place at the micron-scale, against the backdrop of high gradients of residual stresses are developed during the AM process, also known as Type II & Type III RS [14,15]. On the other hand, it is also known that the presence of RS at the macro scale (Type I) can induce distortions [16] and nucleation of thermal cracks [17]. For these reasons RS are an important aspect that is deserved considerable attention.

Besides exploiting the AM technique for the production of whole components, AM has been shown to be very effective for repair of parts and components [18]. AM turns out to be an efficient technology, particularly when the geometry of the target component is rather intricate [19,20]. For example, significant effort has recently been put into the use of this manufacturing method for repairing compressor or turbine blades in energy systems [21], especially where high-performance metallic materials are involved, such as Nickel base superalloy [10,22–26]. Nevertheless, due to the key aspects listed earlier, the limitations and challenges of this manufacturing approach require further research and development. In particular, attention must be paid to the fatigue performance for applications where this represents the most common loading scenario [27]. Most recently, various strategies have been adopted to overcome or control these issues. Some of the most effective ways to improve fatigue properties of these products are through the use of surface enhancement technologies, such as shot peening or laser shock peening [28,29]. These mechanical treatments are capable of introducing compressive residual stress which is well-known to be effective in improving the resistance to fatigue crack nucleation and growth [30], and also in reducing porosity at the near surface region.

It is clear that the combination of microstructure and RS state plays an important role in determining the overall characteristics of the final product's performance in terms of structural integrity. The overall goal of this manufacturing field is the establishment of a technique to produce durable components, which can only be achieved through improved understanding of the damage and failure mechanisms operating in these materials, and the adoption of most appropriate mitigation strategies.

The aim of the present paper is to investigate these matters in an IN718 Ni-base superalloy. For the purpose of the present study, two series of samples produced by Laser Metal Deposition (LMD) technique were analysed, referred to respectively as "A" for the as-AM-printed and "B" for the sample post-processed by shot peening. HCF testing was performed in a vibration bending mode at room temperature on both the samples. In total two samples were tested, which was found to be adequate to study the fracturing and deformation mechanisms in this fatigue regime. In order to investigate the details of the fatigue failure mode, a range of experimental techniques were employed. Firstly, a fractographic study was carried out using Scanning Electron microscopy (SEM) imaging to identify the origins of fatigue crack nucleation, and the propagation mechanisms. In support to this analysis, ElectronBack Scattered Diffraction (EBSD) maps of the grain structure were acquired at different magnifications over the polished fracture surface. Energy Dispersive Spectroscopy (EDX) was also employed to assist chemical composition analysis and phase identification.

Comprehensive experimental RS analysis was conducted in the region of interest, with particularly attention placed on the region where the fatigue failure originated. As a result, the probed region was intrinsically affected by the plastically deformed layer left by the propagating crack during the fatigue test. The analysis of RS is therefore not devoted to the absolute assessment of the RS field induced by the AM and shot peening processes, but rather at evaluating their influence.

The experimental method utilised to accomplish this task was FIB-DIC micro-ring-core milling. This method relies on the synergic use of Focused Ion Beam (FIB), Scanning Electron Microscopy (SEM) and Digital Image Correlation (DIC). In the second instance, after sample sectioning, additional spatially resolved RS line profiling was performed along the direction perpendicular to the crack surface, in order to explore the relationship and interplay between the underlying process-induced porosity, on the one hand, and the RS that persist in the component, on the other. The results gathered from these different techniques are brought together, analysed, and discussed.

2. Sample preparation and methods

2.1. Sample description and preparation

LMD was used for the manufacturing of two sample series made from IN718 Nickel-base Superalloy using blown powder method. The samples were manufactured in the form of a plate of 1.00 mm thickness with rounded edges. Following the AM build process, a thin layer of material was removed around the samples perimeter to reduce the surface roughness and to obtain the desired final shape – the final samples thickness was 0.75 mm and the surface roughness was estimated to be in the order of Ra 1.6-3.2– μm. Sample A series was studied in the as-built and machined condition. Shot peening treatment was applied to Sample B series around the entire contour to induce compressive residual stress at the surface. Table 1 provides a summary of the sample conditions studied in this work.

In the Sample B series, two crack surfaces were generated as a result of the HCF test. One surface was utilised to carry out the fractographic analyses. The second fractured surface was used for the analysis of residual stress. This surface was ground and polished using sand papers of progressively finer grades, up to grit 4000 (equivalent to 5 μm particle size). Further surface polishing was conducted using 3 μm, 1 μm and 0.1 μm diamond suspension. A further surface preparation step was carried out in order to further reduce the impact of sample preparation: etching via a weak acetic acid solution (5 wt%). In this way, the presence

Table 1
Samples description and analyses performed.

Sample series name	Description	Treatments	Tests performed
A (MA2)	As-built	AM + surface machining	Fatigue, RS analysis
B (MAP2)	Shot peened	AM + surface machining + shot peening	Fatigue, fractography, EBSD, FIB-CT, EDX, RS analysis

of residual stress induced by polishing [31] was minimised, along with the enhancement of the local surface contrast for better DIC tracking.

2.2. Methods

2.2.1. High cycle fatigue

The manufactured samples were cyclically loaded in vibration bending mode using a piezoelectric shaker. A laser displacement sensor was used to verify the sample vibration frequency.

The sample was loaded to generate a that peak stress at a specific longitudinal position, where failure occurred . After the sample was HCF tested for 15 min at a pre-determined load amplitude, which was incrementally increased, until a critical condition was attained, and the sample failed. The cyclic load was applied in the direction normal to the longitudinal orientation of the sample, and therefore the resulting bending moment had a linear variation throughout the 0.75 mm of thickness.

2.2.2. FIB-DIC

The assessment of RS conducted in this work was executed by means of the semi-destructive technique called FIB-DIC micro-ring-core milling [32–35]. This method has demonstrated exceptional performance in terms of probing Type I+II+III RS at the micron and even finer scales (down to 50 nm in terms of depth resolution). Given the strain relief occurring in residually stressed materials when a careful cut is performed, a class of FIB and DIC based techniques exploit this effect to back-calculate the stress state prior the material removal [36–39]. In line with this concept, material removal at very small scale is performed using FIB milling with a the precision of a few nanometres. While the material is sequentially removed layer-by-layer, stable and high resolution digital imaging is performed using SEM to acquire a sequence of images of the material surface. The collection of the SEM micrographs are analysed using DIC software to track the displacements at the surface of sample as material removal progresses.

In this work, the FIB material removal process was performed in a ring-core geometry. This particular geometry allows for the extraction and calculation of RS for any in-plane direction [32,40], and is highly suitable for the present study. The diameter of the inner core D generated by the FIB removal was set to 5 μm. DIC analysis was performed over the circular area of $0.8D$ in diameter using a dedicated MATLAB-based software [41], in order to avoid artefacts due to unavoidable FIB damage at the edge of the core [42–44]. The depth of each milling step was set to 100 nm, and the FIB energy used was 30 keV. The milling procedure was stopped when the milled depth reached the value of $0.3D$. It has been shown in the past that strain relief information extracted up to this depth can provide the required input to perform quantitative stress evaluation. The analysis of strain evolution at the surface was carried out for two mutually orthogonal in-plane directions. The final step of the evaluation process allowed the evaluation of residual elastic strain, and the consequent determination of RS. To accomplish this task, the strain relief profiles obtained from each milled point were fitted with a master curve derived from FEM analysis [40,45]. This procedure permitted the quantification of the residual elastic strain, and hence RS, by invoking the appropriate Hooke's law formulation. Each stepwise evaluation of RS in this study was accompanied by detailed error propagation analysis [46,47] based on the uncertainties of DIC tracking; master curve fitting, and local elastic stiffness.

2.2.3. EBSD & EDX

In order to perform grain orientation and chemical composition analyses, the samples were mounted on a 20° pre-tilted holder with the respect of the SEM column axis. EBSD maps were acquired using an electron energy of 15 keV. Thanks to the high quality of the surface finish, high acquisition rate of 6.75 Hz was possible. Low magnification mapping was conducted using the step size of 0.5 μm, while the high magnification mapping step was set to 0.2 μm. Moderate amount of post processing was employed to retrieve unindexed pixels. Where necessary, High Angle Grain Boundaries (HAGB) and Low Angle Grain Boundaries (LAGB) were identified using the adjacent pixel misorientation criteria of 10° and 2.5°, respectively. In the resulting maps, HAGB's were identified by black lines, while LAGB's were represented by grey lines.

EDX analysis was carried out using electron beam energy of 15 keV. Individual maps of the most relevant chemical elements were acquired by cumulative repeated raster scanning until adequate statistical relevance was achieved. For the present analysis, the elements of interest were Ni, Al, Mo, Cr, Fe, Ga, Nb and Ti.

3. Fractography

A detailed analysis of the fractured surface was carried out in the crack nucleation region. SEM image of the fracture surface (Fig. 1a) reveals that intragranular crack propagation mechanisms was predominantly operative. Moreover, numerous faceted surfaced were detected, indicating that the crack propagated by cleavage along preferential crystallographic planes. Similar propagation mechanisms were also observed in the literature for IN718 produced by a Selective Laser Melting (SLM) technique [48]. Notably, discontinuities in these facets were found. These discontinuities are known as “tongues” and can be linked to the microstructure and morphology. As will be later shown in the discussion of Figs. 4 and 5, EBSD maps highlight the presence of parallel bands confined within a single crystal, associated with the formation of twinning during manufacturing. It is therefore possible that the formation of tongues occurs once the crack propagates past the regions of different crystal orientations . It is useful to mention that the presence of such features may be enhanced by the AM process. As shown for Ti-6Al-4V material, the AM method can introduce families of well-arranged grains that induce the formation of these patterns, which were not detected in the wrought version of the same material [49].

Ratchet marks and ridges were found, as shown in Fig. 1(b and c), which aas generally observed, are oriented parallel to the direction of crack growth. Ratchet marks are essentially steps formed where multiple cracks, initially propagating on slightly offset parallel planes, interconnect with each other through secondary cracks running perpendicular to the fracture plane. An example is given by the red dashed line in Fig. 1(b).

Although it is known that fatigue striations can be present in Ni-base superalloys [50], in the present instance these could only be detected sporadically.

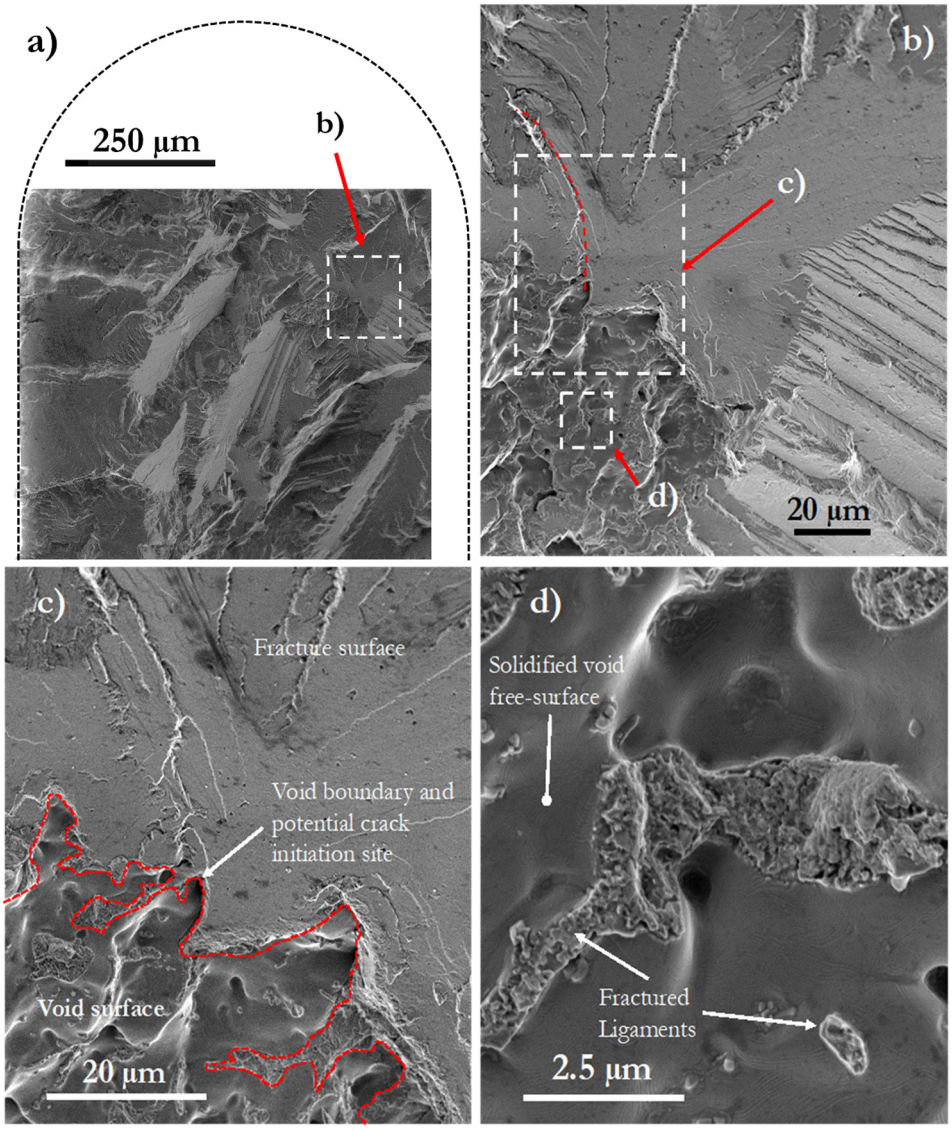

Fig. 1. SEM images of the fractured surface with increased magnification in b), c) and d).

As far as the fatigue crack initiation site is concerned, this could be located within the bulk of the sample, indicated with the white dotted square in Fig. 1(a) and magnified in Fig. 1(b and c). As expected for this type of AM material, crack nucleation occurred close to material defects, in this case voids or cluster of voids. In this specific case-study, Fig. 1(d) shows the defect sharp surface , with some fractured ligaments

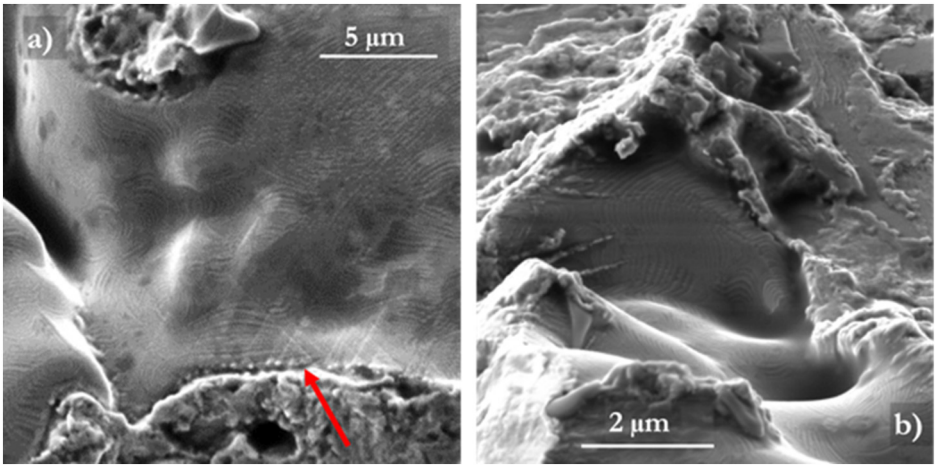

Fig. 2. SEM images of characteristic defect surface features. The arrow in (a) indicates densification of slip bands. (b) defect free-surface morphology.

present, proving that this particular defect can be thought of as a cluster of voids. Additionally, the actual surface of the void appears smooth, hinting that its origin may be gas-entrapment, rather than a lack of fusion [51].

The underlying microstructure is far from continuous, but incorporates void-like defects either due to lack of fusion, i.e. insufficient access of molten material to these sites [52,53], gas entrapment [54], melt pool instability or spatter [17,55].

Although at this stage no secondary cracks were observed running perpendicular to the crack surface [56], it will be shown later that defects of this type were also present within the AM builds, but became visible only upon surface polishing, as illustrated and discussed in the EBSD section (Section 4.1).

The morphology of the void surface is shown in Fig. 2, with the close-up view in Fig. 2(b). It is worth noting curved surface "contour lines" that may be associated with the process of melt solidification during SLM fabrication. These are distinct from straight features that may be associated with underlying deformation mechanisms operative during cooling of solid material, leading to the appearance of extrusions/intrusions, slip or twin bands. Some insights may be obtained by observing the characteristic features pointed out by the red arrow in Fig. 2(a). These parallel and crossing bands can be the associated to the peculiar intrusion/extrusion features that may be induced be the cyclic loading [57] and linked to the deformation occurring along slip planes.

4. EBSD & EDX

4.1. EBSD

Preliminary microstructural characterisation using this EBSD mapping was performed on sample cross-section to reveal the grain morphology along the build direction. As illustrated in the Fig. 3, typical elongated grains were found due to the columnar grain growth operative during solidification, in agreement with the reports in the literature [58].

A more detailed analysis of the underlying microstructure was conducted over the region where the fatigue failure origin was identified. The sample surface was polished as described in the material preparation section to remove the fractured surface. A backscattered electron SEM overview image of the sample is shown in Fig. 4(b). Due to the etching treatment, the phase contrast was enhanced, as can be seen in Fig. 4(a & c). In these micrographs, the presence of the Ni-base solid solution (γ-phase) is indicated by the dark regions, and the bct-Ni_3Nb precipitates, γ″ are the brighter spots; in agreement with the literature reports [59–61].

EBSD mapping was performed in the same region, as shown in Fig. 4(b). The EBSD map (colour on line) reveals the intricate grain morphology present in this cross section of the sample. At the millimetre scale, two main large grains covering the whole map were found, dominated by blue tones on the left-hand side, and green tones on the right-hand side of the map. Nevertheless, discerning the precise grain boundaries presents a challenge due to the presence of multiple internal High-Angle (HAGB) and Low-angle (LAGB) boundaries. Interestingly, the large grain on the left-hand side showed predominantly two large populations of sub-grains: one having orientation coloured in shades of yellow, and the other coloured in shades of green. Each family of sub-grains has the peculiarity of having a lath-like shape, with a similar predominant orientation, and equi-spacing. This pattern suggests that the nucleation of sub-grains may have occurred intragranularly within the main grain at a later stage than the formation of the main large grain. The explanation of these microstructural features lies in the occurrence of material twinning. Relevant literature [62] on this topic reveals that Ni base superalloy displays this deformation mechanism when subjected to creep at elevated temperatures (above about 1050 °C). Other reports found in the literature confirm this behaviour [63,64]. During AM manufacturing, significant stresses arise during workpiece cooling, which makes it likely that the material is subjected to creep loading.

However, deformation twinning may also be operative at the room temperature. Crack nucleation in Ni base superalloys has been reported to occur in regions with a high population of twins [65], both under fatigue and monotonic loading [66]. This aspect is of great interest in the research community studying these materials. In polycrystalline Ni-base superalloys, the origin of fatigue failures is often located at twin boundaries [67]. Fatigue crack nucleation induced by twin deformation is explained in [68], in which twin boundaries are thought of as discontinuities and therefore stress field singularities, with a consequent increase of the local stress. Amplification of the local stress is even more enhanced when the twin lies within the region where stress concentration occurs, e.g. near a notch or a defect. In view of this fact, in this section the attention is also focused at the analysis of the vicinity of the largest defect present in the cross-section, indicated by the red square in Fig. 4(a). According to the fractography analysis presented in the previous section, this defect also corresponds to the crack nucleation site. The close-up EBSD map of the Region of Interest (ROI) is shown in Fig. 4(c). It reveals a high density of the twinning bands discussed above within the neighbourhood of the defect. This is also linked to the high magnitude of RS at his location.

Interestingly, these deformation bands were found more than 30 years ago while examining the Low Cycle Fatigue behaviour of IN 718, and they were recognised to be twins [69,70]. At LCF regime, the

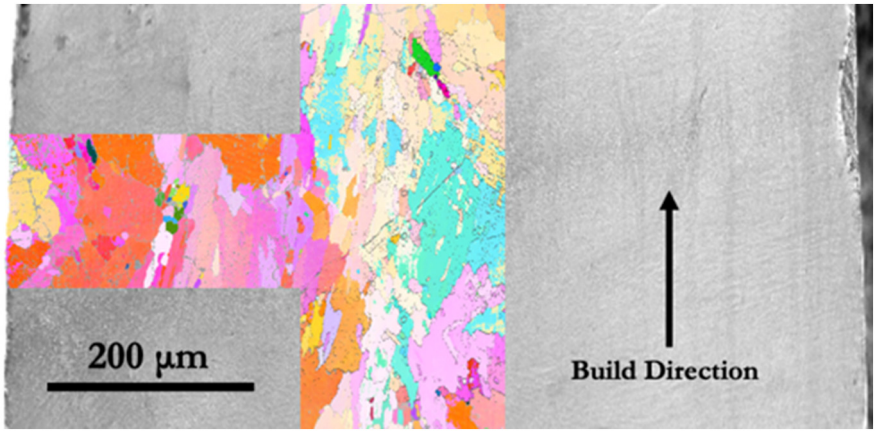

Fig. 3. Vertical section of the sample. Overlapped is the EBSD map (Euler Colour).

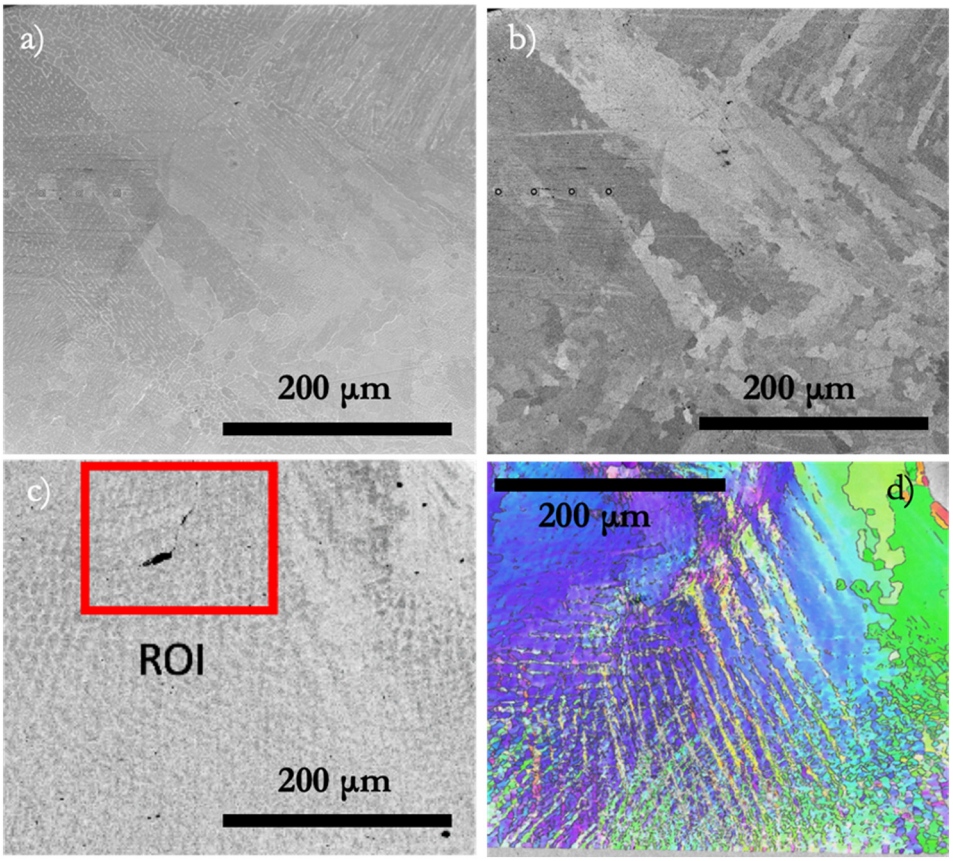

Fig. 4. SEM overview images of the sample cross-sections. (a) and (c) are respectively the Secondary Electron images of the un-fractured and fractured samples. (b) is the BackScattered Electron images of the un-fractured tip highlighting the grain shapes. (d) is the Inverse Pole Figure EBSD map overlapped on SEM image of the fractured sample.

plastic strain is large enough to cause large shear deformation, particularly by shearing the γ″ precipitates in the first instance and then forming the twins. This behaviour also explains the strong directionality of the twin bands found in the EBSD maps. In other words, twin bands develop along the columnar direction of the cellular structure of γ, and therefore also along the γ″. A close-up EBSD map (Fig. 5(c)) from the squared one highlighted in Fig. 5(b), in the region of high deformation density shows the presence of γ″ precipitates (white unindexed regions, circled in red) which correspond to the deformation bands boundaries. It is then evident how these bands are activated during deformation at those locations and develop along these cellular directions.

4.2. EDX

2D map results of the EDX analysis within the region of interest around the investigated defect are shown in Fig. 6. As confirmed quantitatively and reported in Table 2, γ-phase is the predominant phase. The space occupied by this phase can be clearly identified by the regions in the maps shown in Fig. 6, where the concentrations of Mo, Nb and Ti are low. On the other hand, regions showing high concentrations of these listed elements were recognised as γ″-phase. In general, the concentrations listed in Table 2 are in close agreement with the pertinent literature [60], corroborating the phase identification. It is worth noting

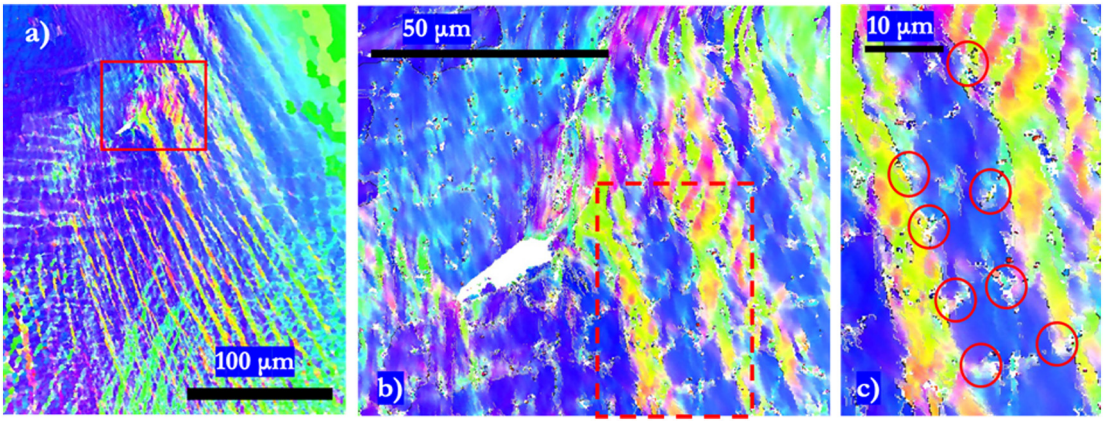

Fig. 5. EBSD Inverse Pole Figure maps of the fractured sample. (a) Overview and region of interest. (b) Close-up at the region of interest. (c) Further close-up at the squared region in (b) with emphasis on the precipitates (circled).

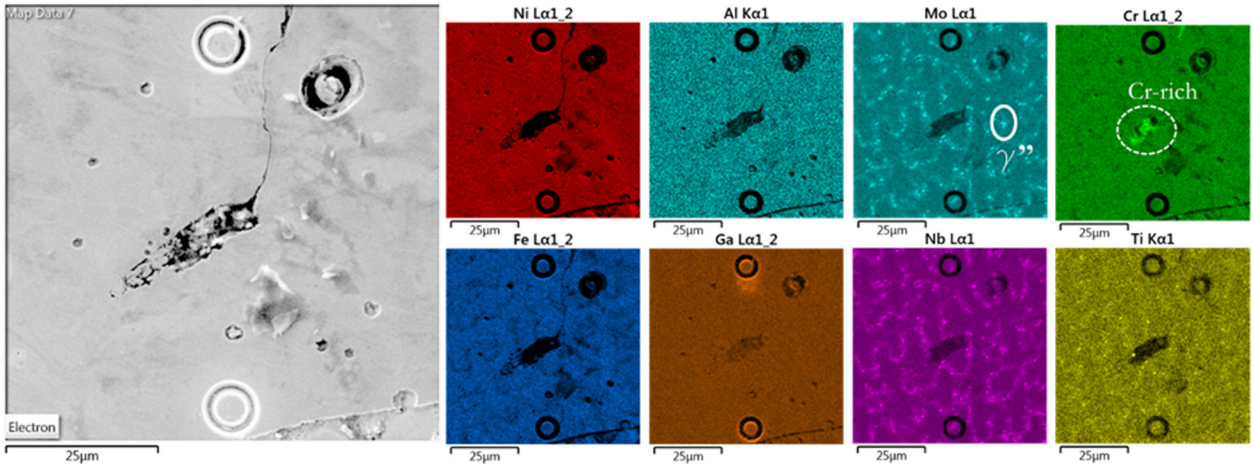

Fig. 6. EDX maps at the region surrounding a large defect.

that the same γ″ phase can be identified in the etched surface BSE images in Fig. 4(a & b).

It is important to mention that the defect's hollow relief causes some attenuation of the outcoming signal. A reduction of the main elemental constituents of IN718 alloy is noted within this defect, with the exception of Gallium and Chromium. Gallium detection was included in the analysis in view of the presence nearby of FIB-DIC micro-ring-cores, also visible in these maps. As expected, elevated concentration of Ga around milling sites was observed. It is also noteworthy to observe an increase of Cr content in the inner regions of the defect. The increase of Cr in Ni base superalloy on the one hand improves the corrosion resistance, for instance as exploited by superalloy IN690, which shows outstanding resistance to oxidising chemicals and to high-temperature oxidising gases. On the other hand, Cr enrichment in a local region reduces the strength of IN718, due to the formation of lower strength Cr-rich phases. It is often surmised that high density of crystal defects such as dislocations can enhance the mass transport of elements through γ matrix, via the so-called pipe diffusion mechanism [71]. Although not verified experimentally, this mechanism may have been active near defects in IN718 samples studied here, leading to Cr segregation [72]. The general reduction in the concentration of Ni, Al, Mo, Ti, Fe and Nb in the defect region may also be associated either with diffusion, or with the increase in local oxidation that occurred during material processing.

5. FIB-DIC residual stress analysis

In order to investigate the role of RS in fatigue performance, a comprehensive campaign of spatially resolved measurements was carried out. The study of RS is important, as they are known to affect the material propensity for crack nucleation and propagation.

Two perpendicular measurement lines were defined according to Fig. 7. The intersection point of the two lines was assumed to be the origin of a Cartesian coordinate system, in which the *x* axis follows the sample section midline. The position of the Cartesian axis *y* on the *x* axis (i.e. origin) was dictated by the position of the relevant feature identified within this cross-section. The purpose of this choice of measurement points was to assess the effects of shot peening treatment from this point of view.

The measured RS profiles are reported in Fig. 8, that shows each line and stress component individually. The measurement results are accompanied by error bars indicating 95% confidence level. Fig. 8(a, c, e, g) refers to the shot peened condition (sample series B). It is clear from the results that high magnitudes of compressive RS were found in the vicinity of the sample free surface. Compressive RS as high as ~1000 MPa are associated with shot peening treatments, the effect of which persists to the depth of ~0.2 mm. At the same locations, RS found in sample series A, depicted in Fig. 8(b, d, f), also showed compressive RS near free surfaces. However, in this case the magnitude of compressive stresses was lower, as well as their extent in depth. It is important to note that shot peened sample manifested a region in the bulk of the sample which contained RS of tensile nature, particularly in the vicinity of the defect of interest. As noted previously [10], in order to satisfy stress equilibrium, compressive residual stresses installed at the free-surface due to shot peening treatment must be balanced throughout the sample thickness. This balance is achieved by the development of tensile residual stress in the inner regions. This highlights the importance of paying particular attention when shot peening is employed for the treatment of thin components. In fact, the amount of the induced inelastic deformation needs to be specially designed for each particular application [10,73,74]. Ignoring these considerations may lead to shot peening weakening the component's fatigue resistance, rather than improving structural performance.

Interestingly, the un-peened sample series (A) does not exhibit the region in which RS is of tensile nature. Fig. 8(b, d, f) shows that regardless the position of spatially resolved measurements of stress components, only compressive RS was found. For this sample, the balance of stresses throughout the sample thickness (Fig. 8(b)) is certainly not verified. This means that the RS distribution in the sample varies across the sample longitudinal direction (in the out-of-plane direction in Fig. 7),

Table 2
Composition of different detected phases and of a relevant area. ND: Non-Detected. For interpretation of the regions, please refer to Figure 6.

Phase/region	Element wt%								
	Ni	Fe	Cr	Nb	Mo	Ti	Al	Cu	Mg
γ	54.9	19.0	19.4	1.9	1.7	0.8	1.1	0.9	0.1
γ″	51.6	13.1	15.7	13.1	2.4	1.9	0.7	0.7	0.3
Cr-rich region	2.5	0.7	63.8	3.8	ND	0.5	ND	13.3	15.4

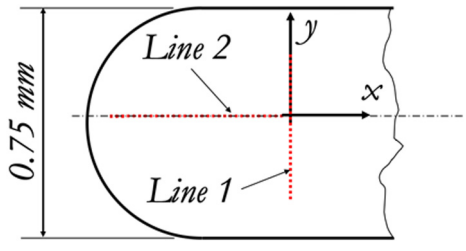

Fig. 7. Overview of the fractured sample and measurement lines.

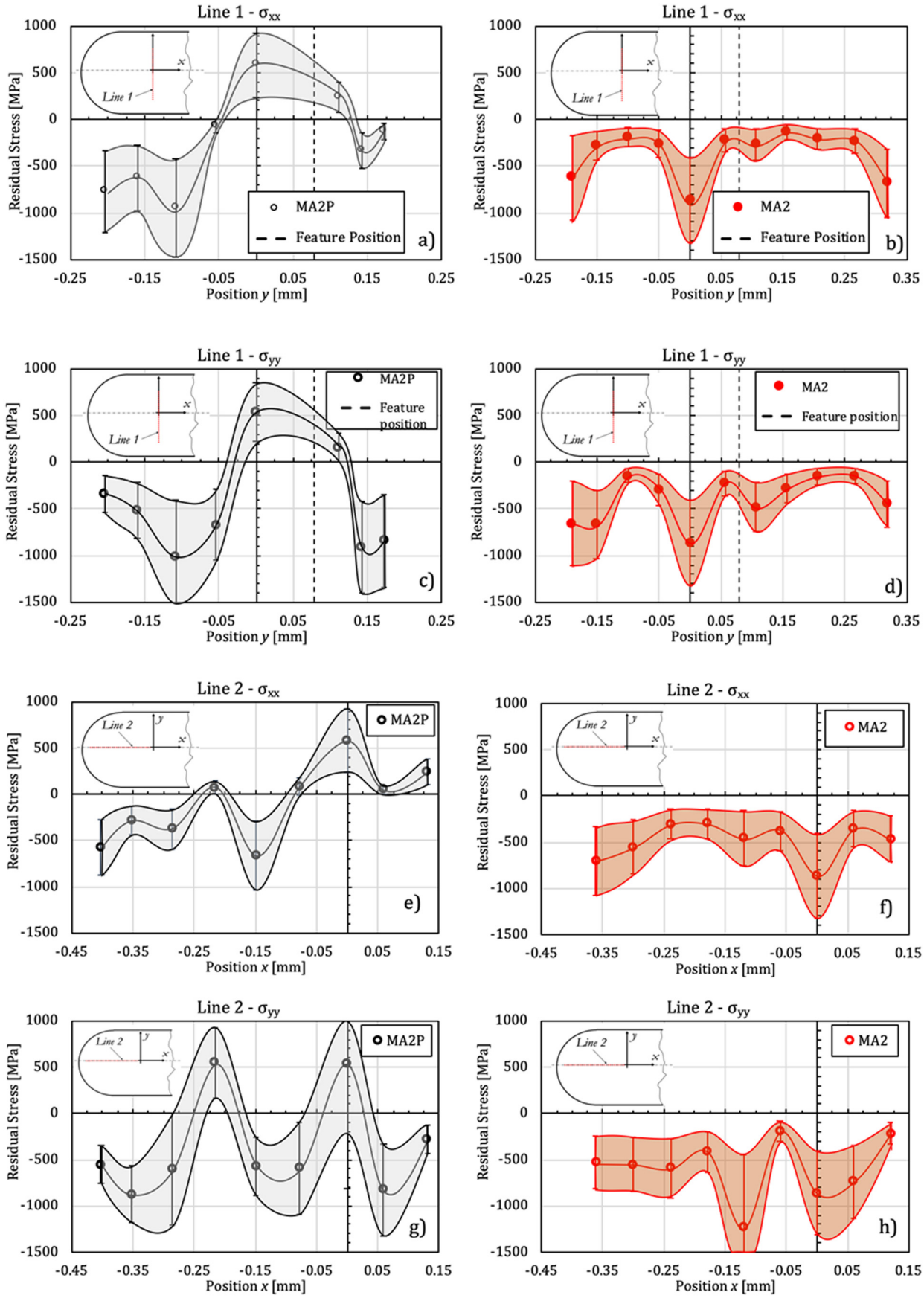

Fig. 8. Residual stress profiles.

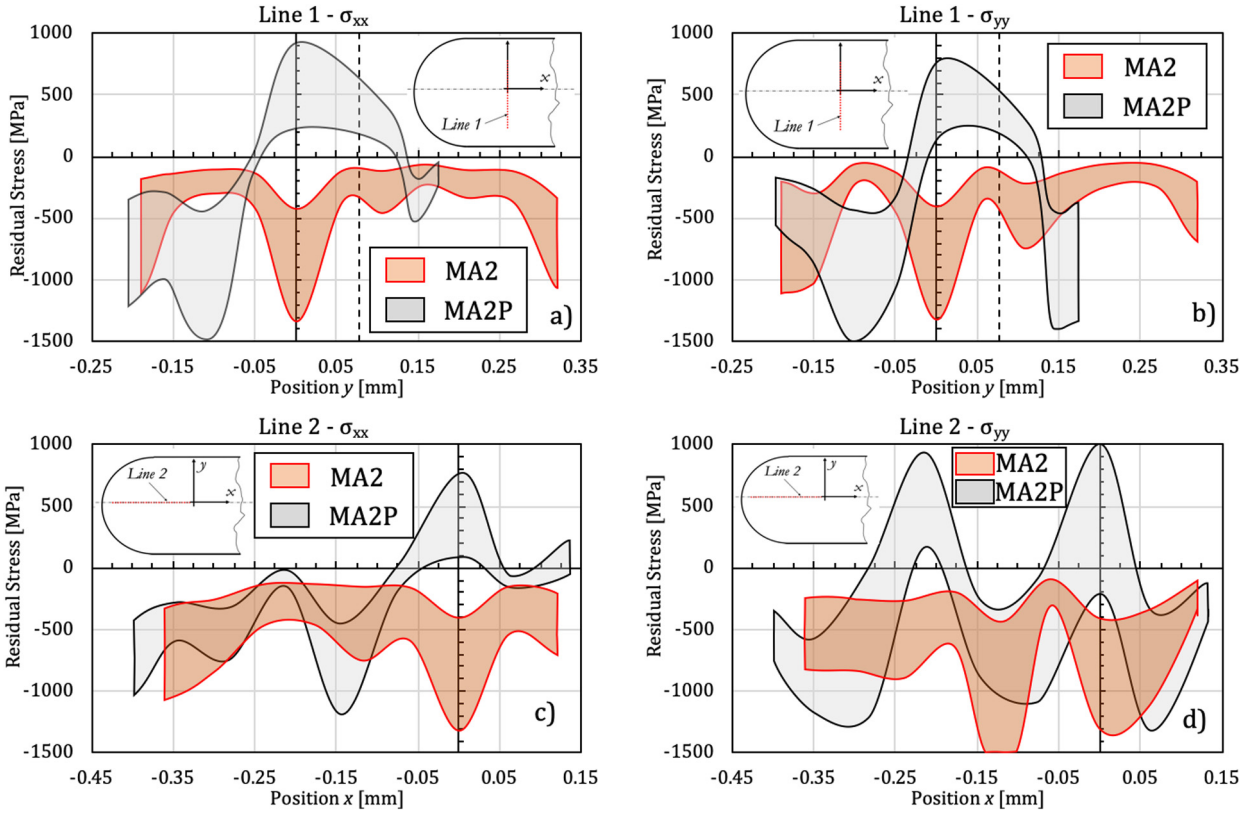

Fig. 9. Residual Stress comparison; Peened vs. Unpeened samples

implying that the manufacturing process generated heterogeneous RS distribution along this direction. Thereby, regions of solely compressive RS must be accompanied by others where tensile RS of a combination of tensile/compressive RS exist.

Despite the possibility that the measurement plane within the two examined sample series were not identical, observations can still be drawn by direct comparison of the profiles, as shown in Fig. 9. This particularly concerns the assessment of shot peening effectiveness. In order to facilitate visualisation and assessment, in these plots the experimental results are shown by means of error bands drawn at the 95% confidence level, as mentioned earlier in the "Methods" section. Shot peening was effective in prescribing extensive compressive RS along "Line 1" for stress component *xx* (or tangential). The same effect could also be noted for "Line 2", for the other component (Fig. 9(d)).

6. General discussion

The comprehensive experimental analysis reported in the present article was used to characterise the microstructure and residual stress state in additively manufactured samples of a IN718 Ni-base superalloy, and to elucidate the fatigue mechanisms operative under cyclic loading. This was accomplished through complementary use of grain structure imaging by SEM and advanced microstructural characterisation techniques (EBSD and EDX).

The examination of fracture surface characteristics provided insight into the origins of fatigue crack nucleation, and its further propagation. Initiation turned out to be strongly affected by the presence of a large defect (or void), and the associated stress amplification. Regarding further crack propagation, the copious presence of 'tongues' and 'ratchets' was noted, associated respectively with crack propagation through twins, and the interaction and confluence of cracks from different parallel propagation planes. To corroborate the twinning deformation mechanism activity during propagation, EBSD maps at different magnifications acquired after polishing of the fractured surface were thoroughly examined. The presence of twin bands was identified, confirming the hypothesis of twinning being the predominant deformation mechanism operative while the fracture progressed. Twin deformation has been reported in the literature in cases when high strain rates were involved [62], indicating that this condition was experienced in the present case during fatigue propagation. This type of mechanism dominates at high strain rates, since slip strain is inhibited within the limited time for deformation to occur, so that twinning becomes the preferred way to deform. It is also worth mentioning that the EBSD maps and BSE images acquired for undeformed microstructure did not detect the presence of twins. It is also well-known that the ease of twinning is closely linked to the stacking fault energy of the alloy [75], although this aspect has not been investigated in the present study. It was further noted that crack nucleation from the defect surface could be additionally promoted by the presence of surface features associated with twins or emerging slip bands that may be thought of as discontinuities giving rise to stress concentration facilitating the nucleation of cracks [64]. Interestingly, similar features were found in the fractographic analysis of HCF tests on wrought IN718 [76], where multisource cleavage-like fracture were observed. However, for the wrought material the principal plastic deformation manner was imputed to the slip deformation and only a limited amount of twinning activity was identified.

Interestingly, EBSD maps at higher magnification revealed the nature of these twin bands. In fact, the clear directional correlation between the cellular structure of γ/γ″ phases and the deformation band suggests that twins were confined, and possibly triggered, by Nb-rich γ″ precipitates. It is worth mentioning that Nb enrichment is thought to have a detrimental effect on material strength.

EDX was performed on the crack initiation site and the surrounding region. Besides revealing the phase composition, EDX highlighted a Cr-rich region associated with the defect. This Cr enrichment is also well-known to be unfavourable from the structural integrity performance point of view.

RS analysis was carried out on the two sample series, namely, shot peened and as-built. While shot peening is known to be effective in introducing compressive RS within the shallowest ~0.2 mm layer of material, it has also been shown to lead to a high magnitude of tensile RS within the bulk of material. Incidentally, the region of high tensile RS was closely associated with the location of the defect at which crack nucleation took place. For the thin plate geometry studied, while the occurrence of crack nucleation was indeed inhibited at the sample surface, at the same time propensity of the crack to nucleate within the bulk was increased. It is important to note that in the as-built sample the presence of high tensile RS was not detected.

7. Conclusions

The analysis carried out in this study has revealed the mechanisms of fatigue crack nucleation and propagation in AM IN718 superalloy samples. A number of phenomena were found to contribute to the initiation and occurrence of fatigue failure:

- The nucleation of fatigue crack was located at the surface of a large internal material defect (i.e. void). Extrusion/intrusion bands were found at the void/material interface, along with a high density of twins. Therefore, both slip and twin deformation modes were operative before crack nucleation.
- Twinning deformation was found to be the dominant deformation mechanism during fatigue crack propagation due to the high local strain rate. The twinning pattern was closely correlated with the distribution and direction of the cellular structure of γ'' precipitates. These precipitates are likely to have a great influence on the occurrence of twins, possibly by obstructing slip deformation.
- A high concentration of Chromium was found at the defect where crack nucleation occurred. Chromium is well-known to improve corrosion resistance, while the strength of Cr-enriched material is known to be reduced.
- RS analysis revealed high magnitudes of grain-level compressive or tensile residual stresses. Interestingly, the shot peened sample exhibited high values of tensile residual stress within the area close to the feature of interest (i.e. defect). It is not possible to state with confidence whether tensile residual stress was present prior to shot peening. Nonetheless, it is clear that shot peening treatment generated additional tensile residual stress in the material bulk. This effect undoubtedly contributed to premature failure initiation far from the free surface.

Data availability

The raw/processed data required to reproduce these findings can be partially shared upon request due to legal reasons and since the data also forms part of an ongoing study.

CRediT authorship contribution statement

Enrico Salvati: Writing - original draft, Methodology, Formal analysis.**Alexander J.G. Lunt:**Methodology.**Chris P. Heason:**Investigation. **Gavin J. Baxter:**Investigation.**Alexander M. Korsunsky:**Writing - original draft.

Acknowledgements

Enrico Salvati would like to acknowledge funding provided by the Engineering and Physical Sciences Research Council EPSRC project EP/P005381/1.

References

[1] W.E. Frazier, Metal additive manufacturing: a review, J. Mater. Eng. Perform. 23 (2014) 1917–1928.
[2] K. Kellens, R. Mertens, D. Paraskevas, W. Dewulf, J.R. Duflou, Environmental impact of additive manufacturing processes: does AM contribute to a more sustainable way of part manufacturing? Procedia CIRP 61 (2017) 582–587.
[3] D. Herzog, V. Seyda, E. Wycisk, C. Emmelmann, Additive manufacturing of metals, Acta Mater. 117 (2016) 371–392.
[4] J.P. Oliveira, T.G. Santos, R.M. Miranda, Revisiting fundamental welding concepts to improve additive manufacturing: from theory to practice, Prog. Mater. Sci. 107 (2020), 100590.
[5] L. Sheridan, O.E. Scott-Emuakpor, T. George, J.E. Gockel, Relating porosity to fatigue failure in additively manufactured alloy 718, Mater. Sci. Eng. A 727 (2018) 170–176.
[6] S. Romano, A. Brückner-Foit, A. Brandão, J. Gumpinger, T. Ghidini, S. Beretta, Fatigue properties of AlSi10Mg obtained by additive manufacturing: defect-based modelling and prediction of fatigue strength, Eng. Fract. Mech. 187 (2018) 165–189.
[7] S. Beretta, S. Romano, A comparison of fatigue strength sensitivity to defects for materials manufactured by AM or traditional processes, Int. J. Fatigue 94 (2017) 178–191.
[8] M. Peron, J. Torgersen, P. Ferro, F. Berto, Fracture behaviour of notched as-built EBM parts: characterization and interplay between defects and notch strengthening behaviour, Theor. Appl. Fract. Mech. 98 (2018) 178–185.
[9] O. Fergani, F. Berto, T. Welo, S.Y. Liang, Analytical modelling of residual stress in additive manufacturing, Fatigue & Fracture of Engineering Materials & Structures 40 (2017) 971–978.
[10] E. Salvati, A.J.G. Lunt, S. Ying, T. Sui, H.J. Zhang, C. Heason, et al., Eigenstrain reconstruction of residual strains in an additively manufactured and shot peened nickel superalloy compressor blade, Comput. Methods Appl. Mech. Eng. 320 (15) (2017) 335–351.
[11] E. Salvati, H. Zhang, K.S. Fong, X. Song, A.M. Korsunsky, Separating plasticity-induced closure and residual stress contributions to fatigue crack retardation following an overload, Journal of the Mechanics and Physics of Solids 98 (2017) 222–235.
[12] E. Salvati, T. Sui, H. Zhang, A.J.G. Lunt, K.S. Fong, X. Song, et al., Elucidating the mechanism of fatigue crack acceleration following the occurrence of an underload, Adv. Eng. Mater. 18 (2016) 2076–2087.
[13] E. Salvati, S. O'Connor, T. Sui, D. Nowell, A.M. Korsunsky, A study of overload effect on fatigue crack propagation using EBSD, FIB–DIC and FEM methods, Eng. Fract. Mech. 167 (2016) 210–223.
[14] E. Salvati, A.M. Korsunsky, An analysis of macro- and micro-scale residual stresses of type I, II and III using FIB-DIC micro-ring-core milling and crystal plasticity FE modelling, Int. J. Plast. 98 (2017) 123–138.
[15] J. Everaerts, E. Salvati, F. Uzun, L. Romano Brandt, H. Zhang, A.M. Korsunsky, Separating macro- (type I) and micro- (type II+III) residual stresses by ring-core FIB-DIC milling and eigenstrain modelling of a plastically bent titanium alloy bar, Acta Mater. 156 (2018) 43–51.
[16] T. Mukherjee, W. Zhang, T. Deb Roy, An improved prediction of residual stresses and distortion in additive manufacturing, Comput. Mater. Sci. 126 (2017) 360–372.
[17] C. Qiu, C. Panwisawas, M. Ward, H.C. Basoalto, J.W. Brooks, M.M. Attallah, On the role of melt flow into the surface structure and porosity development during selective laser melting, Acta Mater. 96 (2015) 72–79.
[18] M. Leino, J. Pekkarinen, R. Soukka, The role of laser additive manufacturing methods of metals in repair, refurbishment and remanufacturing–enabling circular economy, Phys. Procedia 83 (2016) 752–760.
[19] X. Zhang, W. Li, K.M. Adkison, F. Liou, Damage reconstruction from tri-dexel data for laser-aided repairing of metallic components, Int. J. Adv. Manuf. Technol. 96 (2018) 3377–3390.
[20] X. Zhang, W. Li, X. Chen, W. Cui, F. Liou, Evaluation of component repair using direct metal deposition from scanned data, Int. J. Adv. Manuf. Technol. 95 (2018) 3335–3348.
[21] J. Gao, X. Chen, O. Yilmaz, N. Gindy, An integrated adaptive repair solution for complex aerospace components through geometry reconstruction, Int. J. Adv. Manuf. Technol. 36 (2008) 1170–1179.
[22] Y. Zhao, J. Sun, Z. Jia, W. Cheng, J. Wang, Research on laser additive and milling subtractive composite remanufacturing process of compressor blade, Journal of Manufacturing and Materials Processing 2 (2018) 73.
[23] C. Zhong, J. Kittel, A. Gasser, J.H. Schleifenbaum, Study of nickel-based super-alloys Inconel 718 and Inconel 625 in high-deposition-rate laser metal deposition, Opt. Laser Technol. 109 (2019) 352–360.
[24] K. Yuan, W. Guo, P. Li, Y. Zhang, X. Li, X. Lin, Thermomechanical behavior of laser metal deposited Inconel 718 superalloy over a wide range of temperature and strain rate: testing and constitutive modeling, Mech. Mater. 135 (2019) 13–25.
[25] X. Ni, L. Zhang, W. Wu, D. Zhu, D. Kong, C. Dong, et al., Functionally Nb graded inconel 718 alloys fabricated by laser melting deposition: mechanical properties and corrosion behavior, Anti-Corrosion Methods and Materials 67 (2020) 16–23.
[26] D. Kong, C. Dong, X. Ni, L. Zhang, C. Man, G. Zhu, et al., Effect of TiC content on the mechanical and corrosion properties of Inconel 718 alloy fabricated by a high-throughput dual-feed laser metal deposition system, J. Alloys Compd. 803 (2019) 637–648.
[27] M. Benedetti, V. Fontanari, M. Bandini, F. Zanini, S. Carmignato, Low- and high-cycle fatigue resistance of Ti-6Al-4V ELI additively manufactured via selective laser melting: mean stress and defect sensitivity, Int. J. Fatigue 107 (2018) 96–109.
[28] S. Luo, W. He, K. Chen, X. Nie, L. Zhou, Y. Li, Regain the fatigue strength of laser additive manufactured Ti alloy via laser shock peening, J. Alloys Compd. 750 (2018) 626–635.

[29] Z. Xu, J. Dunleavey, M. Antar, R. Hood, S.L. Soo, G. Kucukturk, et al., The influence of shot peening on the fatigue response of Ti-6Al-4V surfaces subject to different machining processes, Int. J. Fatigue 111 (2018) 196–207.
[30] M. Benedetti, V. Fontanari, B.D. Monelli, Plain fatigue resistance of shot peened high strength aluminium alloys: effect of loading ratio, Procedia Engineering 2 (2010) 397–406.
[31] J. Everaerts, E. Salvati, A.M. Korsunsky, Nanoscale depth profiling of residual stresses due to fine surface finishing, Adv. Mater. Interfaces 6 (2019), 1900947.
[32] E. Salvati, L. Romano-Brandt, M.Z. Mughal, M. Sebastiani, A.M. Korsunsky, Generalised residual stress depth profiling at the nanoscale using focused ion beam milling, Journal of the Mechanics and Physics of Solids 125 (2019) 488–501.
[33] A.M. Korsunsky, E. Salvati, A.G.J. Lunt, T. Sui, M.Z. Mughal, R. Daniel, et al., Nanoscale residual stress depth profiling by focused ion beam milling and eigenstrain analysis, Mater. Des. 145 (2018) 55–64.
[34] E. Salvati, A.M. Korsunsky, Micro-scale measurement & FEM modelling of residual stresses in AA6082-T6 Al alloy generated by wire EDM cutting, J. Mater. Process. Technol. 275 (2020), 116373.
[35] E. Salvati, J. Everaerts, K. Kageyama, A.M. Korsunsky, Transverse fatigue behaviour and residual stress analyses of double sided FSW aluminium alloy joints, Fatigue & Fracture of Engineering Materials & Structures 42 (2019) 1980–1990.
[36] B. Winiarski, P.J. Withers, Mapping residual stress profiles at the micron scale using FIB micro-hole drilling, Appl. Mech. Mater. (2010) 267–272.
[37] M. Krottenthaler, C. Schmid, J. Schaufler, K. Durst, M. Göken, A simple method for residual stress measurements in thin films by means of focused ion beam milling and digital image correlation, Surf. Coat. Technol. 215 (2013) 247–252.
[38] G.S. Schajer, B. Winiarski, P.J. Withers, Hole-drilling residual stress measurement with artifact correction using full-field DIC, Exp. Mech. 53 (2013) 255–265.
[39] M. Krottenthaler, L. Benker, M.Z. Mughal, M. Sebastiani, K. Durst, M. Göken, Effect of elastic anisotropy on strain relief and residual stress determination in cubic systems by FIB-DIC experiments, Mater. Des. 112 (2016) 505–511.
[40] A.J.G. Lunt, E. Salvati, L. Ma, I.P. Dolbyna, T.K. Neo, A.M. Korsunsky, Full in-plane strain tensor analysis using the microscale ring-core FIB milling and DIC approach, Journal of the Mechanics and Physics of Solids 94 (2016) 47–67.
[41] M. Senn, Digital Image Correlation and Tracking. [Computer Software], https://uk.mathworks.com/matlabcentral/fileexchange/50994-digital-image-correlation-and-tracking 2015.
[42] A.M. Korsunsky, J. Guénolé, E. Salvati, T. Sui, M. Mousavi, A. Prakash, et al., Quantifying eigenstrain distributions induced by focused ion beam damage in silicon, Mater. Lett. 185 (2016) 47–49.
[43] E. Salvati, T. Sui, A.J.G. Lunt, A.M. Korsunsky, The effect of eigenstrain induced by ion beam damage on the apparent strain relief in FIB-DIC residual stress evaluation, Mater. Des. 92 (2016) 649–658.
[44] E. Salvati, L.R. Brandt, C. Papadaki, H. Zhang, S.M. Mousavi, D. Wermeille, et al., Nanoscale structural damage due to focused ion beam milling of silicon with Ga ions, Mater. Lett. 213 (2018) 346–349.
[45] A.J.G. Lunt, N. Baimpas, E. Salvati, I.P. Dolbnya, T. Sui, S. Ying, et al., A state-of-the-art review of micron-scale spatially resolved residual stress analysis by FIB-DIC ring-core milling and other techniques, The Journal of Strain Analysis for Engineering Design 50 (2015) 426–444.
[46] A.J.G. Lunt, A.M. Korsunsky, A review of micro-scale focused ion beam milling and digital image correlation analysis for residual stress evaluation and error estimation, Surf. Coat. Technol. 283 (2015) 373–388.
[47] E. Salvati, T. Sui, A.M. Korsunsky, Uncertainty quantification of residual stress evaluation by the FIB-DIC ring-core method due to elastic anisotropy effects, Int. J. Solids Struct. 87 (2016) 61–69.
[48] Y. Yamashita, T. Murakami, R. Mihara, M. Okada, Y. Murakami, Defect analysis and fatigue design basis for Ni-based superalloy 718 manufactured by selective laser melting, Int. J. Fatigue 117 (2018) 485–495.
[49] S.M.J. Razavi, F. Berto, Directed energy deposition versus wrought Ti-6Al-4V: a comparison of microstructure, fatigue behavior, and notch sensitivity, Adv. Eng. Mater. 21 (2019), 1900220.
[50] Z.H. Jiao, L.M. Lei, H.C. Yu, F. Xu, R.D. Xu, X.R. Wu, Experimental evaluation on elevated temperature fatigue and tensile properties of one selective laser melted nickel based superalloy, Int. J. Fatigue 121 (2019) 172–180.
[51] A.T. Polonsky, M.P. Echlin, W.C. Lenthe, R.R. Dehoff, M.M. Kirka, T.M. Pollock, Defects and 3D structural inhomogeneity in electron beam additively manufactured Inconel 718, Mater. Charact. 143 (2018) 171–181.
[52] K. Solberg, F. Berto, Notch-defect interaction in additively manufactured Inconel 718, Int. J. Fatigue 122 (2019) 35–45.
[53] C. Qiu, N.J.E. Adkins, M.M. Attallah, Microstructure and tensile properties of selectively laser-melted and of HIPed laser-melted Ti-6Al-4V, Mater. Sci. Eng. A 578 (2013) 230–239.
[54] T. Vilaro, C. Colin, J.D. Bartout, As-fabricated and heat-treated microstructures of the Ti-6Al-4V alloy processed by selective laser melting, Metallurgical and Materials Transactions A: Physical Metallurgy and Materials Science 42 (2011) 3190–3199.
[55] C. Qiu, S. Yue, N.J.E. Adkins, M. Ward, H. Hassanin, P.D. Lee, et al., Influence of processing conditions on strut structure and compressive properties of cellular lattice structures fabricated by selective laser melting, Mater. Sci. Eng. A 628 (2015) 188–197.
[56] R. Konečná, L. Kunz, G. Nicoletto, A. Bača, Long fatigue crack growth in Inconel 718 produced by selective laser melting, Int. J. Fatigue 92 (2016) 499–506.
[57] J. Polák, V. Mazánová, M. Heczko, R. Petráš, I. Kuběna, L. Casalena, et al., The role of extrusions and intrusions in fatigue crack initiation, Eng. Fract. Mech. 185 (2017) 46–60.
[58] H. Helmer, A. Bauereiß, R.F. Singer, C. Körner, Grain structure evolution in Inconel 718 during selective electron beam melting, Mater. Sci. Eng. A 668 (2016) 180–187.
[59] J. Belan, High frequency fatigue test of in 718 alloy – microstructure and fractography evaluation, Metalurgija 54 (2015) 59–62.
[60] A. Mostafa, I.P. Rubio, V. Brailovski, M. Jahazi, M. Medraj, Structure, texture and phases in 3D printed IN718 alloy subjected to homogenization and HIP treatments, Metals 7 (2017).
[61] W.M. Tucho, P. Cuvillier, A. Sjolyst-Kverneland, V. Hansen, Microstructure and hardness studies of Inconel 718 manufactured by selective laser melting before and after solution heat treatment, Mater. Sci. Eng. A 689 (2017) 220–232.
[62] J.B. le Graverend, F. Pettinari-Sturmel, J. Cormier, M. Hantcherli, P. Villechaise, J. Douin, Mechanical twinning in Ni-based single crystal superalloys during multiaxial creep at 1050 °C, Mater. Sci. Eng. A 722 (2018) 76–87.
[63] X. Fan, Z. Guo, X. Wang, J. Yang, J. Zou, Grain refinement of a powder nickel-base superalloy using hot deformation and slow-cooling, Materials 11 (2018).
[64] D. Barba, E. Alabort, S. Pedrazzini, D.M. Collins, A.J. Wilkinson, P.A.J. Bagot, et al., On the microtwinning mechanism in a single crystal superalloy, Acta Mater. 135 (2017) 314–329.
[65] J.R. Yates, W. Zhang, K.J. Miller, The initiation and propagation behaviour of short fatigue cracks in Waspaloy subjected to bending, Fatigue & Amp; Fracture of Engineering Materials & Amp; Structures 16 (1993) 351–362.
[66] L. Kovarik, R.R. Unocic, J. Li, P. Sarosi, C. Shen, Y. Wang, et al., Microtwinning and other shearing mechanisms at intermediate temperatures in Ni-based superalloys, Prog. Mater. Sci. 54 (2009) 839–873.
[67] S.R. Yeratapally, M.G. Glavicic, M. Hardy, M.D. Sangid, Microstructure based fatigue life prediction framework for polycrystalline nickel-base superalloys with emphasis on the role played by twin boundaries in crack initiation, Acta Mater. 107 (2016) 152–167.
[68] F. Sun, J. Zhang, H. Harada, Deformation twinning and twinning-related fracture in nickel-base single-crystal superalloys during thermomechanical fatigue cycling, Acta Mater. 67 (2014) 45–57.
[69] D. Fournier, A. Pineau, Low cycle fatigue behavior of Inconel 718 at 298 K and 823 K, Metall. Trans. A. 8 (1977) 1095–1105.
[70] M. Clavel, A. Pineau, Fatigue behaviour of two nickel-base alloys I: experimental results on low cycle fatigue, fatigue crack propagation and substructures, Mater. Sci. Eng. 55 (1982) 157–171.
[71] R. Giraud, Z. Hervier, J. Cormier, G. Saint-Martin, F. Hamon, X. Milhet, et al., Strain effect on the γ′ dissolution at high temperatures of a nickel-based single crystal superalloy, Metallurgical and Materials Transactions A: Physical Metallurgy and Materials Science 44 (2013) 131–146.
[72] P. Kontis, Z. Li, D.M. Collins, J. Cormier, D. Raabe, B. Gault, The effect of chromium and cobalt segregation at dislocations on nickel-based superalloys, Scr. Mater. 145 (2018) 76–80.
[73] A. Vasu, R.V. Grandhi, Effects of curved geometry on residual stress in laser peening, Surf. Coat. Technol. 218 (2013) 71–79.
[74] E. Salvati, A.M. Korsunsky, A simplified FEM Eigenstrain residual stress reconstruction for surface treatments in arbitrary 3D geometries, Int. J. Mech. Sci. 138–139 (2018)Pages 457-466.
[75] I.S. Kim, B.G. Choi, H.U. Hong, Y.S. Yoo, C.Y. Jo, Anomalous deformation behavior and twin formation of Ni-base superalloys at the intermediate temperatures, Mater. Sci. Eng. A 528 (2011) 7149–7155.
[76] L. Zhong, H. Hu, Y. Liang, C. Huang, High cycle fatigue performance of inconel 718 alloys with different strengths at room temperature, Metals 9 (2018) 13.